Detection and Correction of AMSR-E Radio-Frequency Interference*

WU Ying[1,2†](吴 莹) and WENG Fuzhong[3](翁富忠)

1 *Center of Data Assimilation for Research and Application, Nanjing University of Information Science & Technology, Nanjing* 210044, *China*

2 *School of Remote Sensing, Nanjing University of Information Science & Technology, Nanjing* 210044, *China*

3 *NOAA/NESDIS/Center for Satellite Application and Research, Camp Springs, MD* 20746, *USA*

(Received May 31, 2010; in final form April 14, 2011)

ABSTRACT

Radio-frequency interference (RFI) affects greatly the quality of the data and retrieval products from space-borne microwave radiometry. Analysis of the Advanced Microwave Scanning Radiometer on the Earth Observing System (AMSR-E) Aqua satellite observations reveals very strong and widespread RFI contaminations on the C- and X-band data. Fortunately, the strong and moderate RFI signals can be easily identified using an index on observed brightness temperature spectrum. It is the weak RFI that is difficult to be separated from the nature surface emission. In this study, a new algorithm is proposed for RFI detection and correction. The simulated brightness temperature is used as a background signal (B) and a departure of the observation from the background (O–B) is utilized for detection of RFI. It is found that the O–B departure can result from either a natural event (e.g., precipitation or flooding) or an RFI signal. A separation between the nature event and RFI is further realized based on the scattering index (SI). A positive SI index and low brightness temperatures at high frequencies indicate precipitation. In the RFI correction, a relationship between AMSR-E measurements at 10.65 GHz and those at 18.7 or 6.925 GHz is first developed using the AMSR-E training data sets under RFI-free conditions. Contamination of AMSR-E measurements at 10.65 GHz is then predicted from the RFI-free measurements at 18.7 or 6.925 GHz using this relationship. It is shown that AMSR-E measurements with the RFI-correction algorithm have better agreement with simulations in a variety of surface conditions.

Key words: radio-frequency interference (RFI), RFI index, RFI detection

Citation: Wu Ying and Weng Fuzhong, 2011: Detection and correction of AMSR-E radio-frequency interference. *Acta Meteor. Sinica*, **25**(5), 669–681, doi: 10.1007/s13351-011-0510-0.

1. Introduction

Observations from passive microwave sensors onboard satellites provide information about the earth and the atmospheric states under all weather conditions. Measurements over oceans can be used for retrievals of sea surface temperature (SST) and sea surface wind (SSW) as well as atmospheric total cloud liquid water content, water vapor and precipitation (Wilheit et al., 2003). Over land, measurements at low frequencies are usually used to retrieve land surface parameters such as soil moisture, vegetation water content, surface temperature (Njoku and Li, 1999; Njoku et al., 2000), and snow cover (Kelly et al., 2003). Evaluations of different approaches that have been used to derive land surface parameters from C-band Advanced Microwave Scanning Radiometer on the Earth Observing System (AMSR-E) and other passive satellite observations can be found in Njoku and Li (1999), Paloscia et al. (2001), Owe et al. (2001), Njoku et al. (2003), and Chauhan et al. (2003).

Recently, there exists an increased attention from both the scientific and commercial users of the radio spectrum to the radio-frequency interference (RFI) problem, which affects passive and active microwave sensing of the earth from space. RFI, if not properly

*Supported by the National Key Basic Research and Development (973) Program of China (2010CB951600), National Natural Science Foundation of China (40875015, 40875016, and 40975019), Special Fund for University Doctoral Students of China (20060300002), Chinese Academy of Meteorological Sciences "Application of Meteorological Data in GRAPES-3DVar" Program, and NOAA/NESDIS/Center for Satellite Applications and Research (STAR) CalVal Program.

†Corresponding author: wuying_nuist@163.com.

identified, could significantly reduce the scientific value of existing and future C- and X-band passive microwave missions. Because of the presence of RFI signals at AMSR-E 6.925 GHz, this channel was not used for the retrieval of soil moisture over land (Li et al., 2004; Chauhan et al., 2003). Without the measurements at 6.925 GHz, the algorithm sensitivity is significantly reduced and the quality of soil moisture product reduces, especially over dense vegetation areas.

In this study, an algorithm is proposed and tested for detecting AMSR-E RFI signals and correcting RFI contaminated data. In Section 2, a brief description of AMSR-E data and data acquisition is provided. A methodology for detecting the RFI phenomenon and its spatial distribution is presented in Section 3. Correction for RFI contaminated data is given in Section 4. In Section 5, the summary and coclusions are provided.

2. AMSR-E data

The AMSR was developed and provided by the Japan Aerospace Exploration Agency (JAXA) under the contract with Mitsubishi Electric Corporation (Kawanishi et al., 2003). It is onboard the National Aeronautics and Space Administration (NASA) Earth Observing System (EOS) Aqua satellite which was launched on 4 May 2002.

AMSR-E is a 12-channel and 6-frequency passive-microwave radiometer system. It measures horizontally and vertically polarized brightness temperatures at 6.925, 10.65, 18.7, 23.8, 36.5, and 89.0 GHz. The spatial resolution of the individual measurements decreases from 5.4 km at 89 GHz to 56 km at 6.9 GHz. From Aqua's 705-km orbit, the antenna conically scans the earth at a 47.4° angle which corresponds to a local earth incidence angle of 55°. Satellite azimuthally scans within ±61° off the nadir and therefore provides an observational swath width of 1445 km. Since it orbits around the earth in a sun-synchronous mode, its equator crossing time is at 1:30 am and 1:30 pm (local time) in its descending and ascending mode, respectively. Other parameters on radiometer and antenna characteristics are listed in Table 1.

In comparison with the past microwave radiometers (e.g., Scanning Multichannel Microwave Radiometer (SMMR) and Special Sensor Microwave/Imager (SSM/I)), the AMSR-E has an improved spatial resolution and combines the channels of SMMR and those of SSM/I in a single platform.

Table 1. Aqua AMSR-E characteristics

Center frequencies (GHz)	6.925	10.65	18.7	23.8	36.5	89.0
Band designation	C	X	K	K	Ka	w
Bandwidth (MHz)	350	100	200	400	1000	3000
Lower range (GHz)	6.750	10.60	18.6	23.6	36.6	87.5
Higher range (GHz)	7.100	10.70	18.8	24.0	37.0	90.5
Sensitivity (K)	0.3	0.6	0.6	0.6	0.6	1.1
Instantaneous FOV (km)	75×43	51×30	27×16	31×18	14×8	6×4
Sampling (km)	10×10	10×10	10×10	10×10	10×10	5×5
Integration time ($\times10^6$ s)	2.6	2.6	2.6	2.6	2.6	1.3
Main beam efficiency (%)	95.3	95.0	96.3	96.4	95.3	96.0
Beamwidth (degree)	2.2	1.4	0.8	0.9	0.4	0.18

AMSR-E radiance and products processing are carried out by the Remote Sensing System (RSS) in Santa Rosa, California. Level-1A data are received from JAXA via the NASA Jet Propulsion Laboratory (JPL) Physical Oceanography Distributed Active Archive Center (PODAAC). The level-1A data contain sensor counts and coefficients required for computing antenna temperatures and, subsequently, surface brightness temperatures at level-1B. RSS also generates a level-2A re-sampled brightness temperature product and transmits it via ftp to the Global Hydrology Climate Center (GHCC) AMSR-E Science Investigator-led Processing System (SIPS). The SIPS has two components, one located at the RSS facility in Santa Rosa, California, and the other at the GHCC in

Huntsville, Alabama. The AMSR-E SIPS team then further processes the level-2A data into level-2B swath products and then into level-3 daily, 5-day, weekly, and monthly gridded products. The level-2A, -2B, -3 products, the associated metadata, product history, quality assurance files, ancillary files, and Delivery Algorithm Packages (DAPS) are finally transferred to the National Snow and Ice Data Center (NSIDC) Distributed Active Archive Center (DAAC) for archival and distribution to users.

3. RFI detection

An extensive RFI at the 6.925-GHz brightness temperature data from AMSR-E instrument was noticed earlier by Li et al. (2004). RFI contamination at 6.925 GHz increases the channel brightness temperatures. The natural phenomenon such as flooding and wet surface decreases the brightness temperatures at this channel. Man-made radiation from active microwave transmitters (or RFI to a radiometer) is distinctly different from natural radiation in terms of intensity, spatial variability, spectral characteristics, and channel correlations. RFI signals typically arise from a wide variety of coherent point target sources, i.e., radiating devices and antennas, and are often directional, isolated, narrowbanded, and coherent. On the other hand, the earth's surfaces often produce smooth, ultra-widebanded, and incoherent microwave radiation. At and below 30 GHz, scattering effects from natural targets are relatively weaker than the emission signals. RFI can increase brightness temperatures significantly at a particular frequency and generate a negative spectral gradient (Li et al., 2004).

Using the Community Radiative Transfer Model (CRTM), we can simulate the natural correlation between AMSR-E 6.925 and 10.65 GHz and use it for RFI detection and correction of RFI contamination. The CRTM is developed at the US Joint Center for Satellite Data Assimilation (JCSDA). It simulates the microwave and infrared radiances observed by instruments onboard spacecraft for a given state of the atmosphere and earth's surface. It includes components that compute the gaseous absorption of radiation, absorption and scattering of radiation by hydrometeors and aerosols, and emission and reflection of radiation by ocean, land, snow, and ice surfaces. In this study, the surface parameters such as canopy water content, soil moisture content, and skin and soil temperatures required by CRTM, come from the National Centers for Environmental Prediction (NCEP) Global Data Assimilation system (GDAS) outputs. Currently, the NCEP GDAS produces analyses of atmospheric profiles four times a day after assimilating all the radiosonde and satellite data in its global forecast system (GFS) in each cycle. Over the areas where the radiosonde measurements are sparsely distributed or not available, the GDAS produces the analyses based on mostly satellite observations and numerical weather prediction model forecasts. In this study, GDAS data are collocated with AMSR-E in its orbital file format by interpolation in space and time.

Figures 1a and 1b show the scatter plots of simulated (Fig. 1a) and observed (Fig. 1b) brightness temperatures at 6.925 and 10.65 GHz, respectively. The green and pink points in Fig. 1b are likely contaminated by microwave radio frequency transmission. The observed horizontally and vertically polarized brightness temperatures are above 310 and 320 K, respectively, arising from the additional emissions from man-made sources (Fig. 1b). These outliers are not found in model simulations (Fig. 1a). Therefore, the observational departures from model simulations are large in the presence of RFI contamination.

Figure 2 displays the relationship of simulated (Fig. 2a) and observed (Fig. 2b) brightness temperatures between 10.65 and 18.7 GHz. It is seen that the observed brightness temperatures at 18.7 GHz do not display anomalous features. Contamination above 290 K in horizontally polarized channel and 310 K in vertically polarized channel is evident at 10.65 GHz, but not in 18.7 GHz (Fig. 2b). As long as the RFI does not occur in all channels, empirical algorithms can be developed using their natural channel correlation. Li et al. (2004) proposed an RFI index to identify the location of RFI and quantify its intensity:

$$\mathrm{RFI}_{p,f_1} = \mathrm{TB}_{p,f_1} - \mathrm{TB}_{p,f_2}, \tag{1}$$

where TB denotes brightness temperature, the

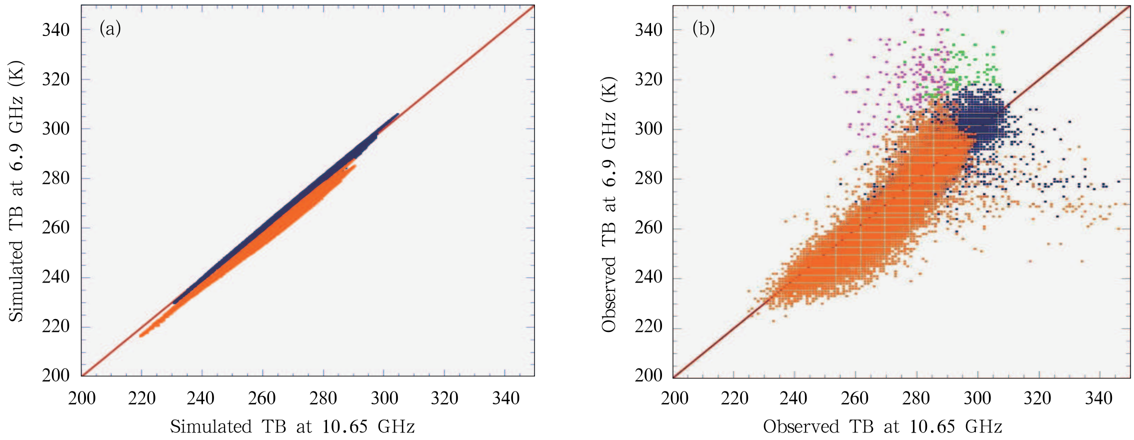

Fig. 1. (a) Simulated and (b) observed brightness temperature relationships between 6.925 and 10.65 GHz. The green and pink points are RFI contaminated data. The AMSR-E data are obtained from Aqua AMSR-E over the continental United States (land only) on 3 October 2008. The blue and green points are for vertical polarization, and the orange and pink points are for horizontal polarization.

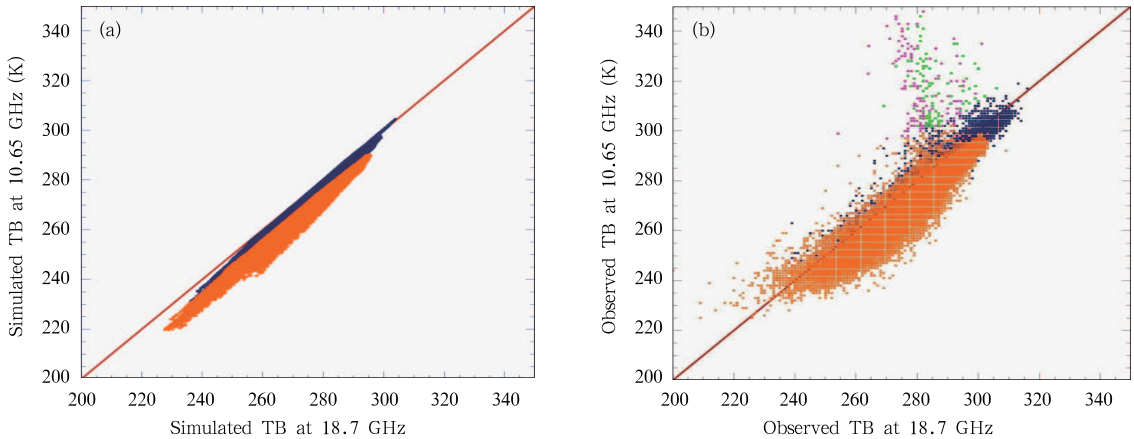

Fig. 2. (a) Simulated and (b) observed brightness temperature relationships between 10.65 and 18.7 GHz. The green and pink points are RFI contaminated data, The AMSR-E data are obtained from Aqua AMSR-E over the Europe (land only) on 3 October 2008. The blue and green points are for vertical polarization, and the orange and pink points are for horizontal polarization.

subscript p stands for horizontal or vertical polarization, and f_1 and f_2 represent the two neighborhood frequencies ($f_1 \leqslant f_2$).

At 6.925 GHz, water bodies (e.g., ocean or lakes) have very low emissions, resulting in brightness temperatures as low as 70 K with horizontal polarization and 170 K with vertical polarization. Land surfaces have a generally higher emissivity, resulting in brightness temperatures in the range as high as 250–320 K. The present of brightness temperature of about 350 K (Figs. 1b and 2b) in the horizontally and vertically polarized channels associated with RFI contamination seems to be the high brightness temperature due to anthropogenic sources. At 10.65 GHz, the passive microwave response to the surface features is similar to that at 6.925 GHz, with water bodies having low brightness temperatures while the land areas high brightness temperatures. Thus, a coastline mask has been applied to remove data over oceanic and large inland water regions (Figs. 1b and 2b). It is emphasized that land brightness temperatures near the coastlines could be influenced by ocean emission viewed by the antenna side lobes.

The AMSR-E brightness temperatures over most land surfaces display a distinct frequency-dependence (e.g., spectrum). The brightness temperature at 10.65 GHz is usually higher than that at 6.925 GHz, which is caused by the spectral dielectric properties of soil and water mixture. The negative values for RFI_{h6} and RFI_{v6} (see Eq. (1)) indicate a normal condition without RFI contamination. A large and positive value of RFI_{h6}, RFI_{v6}, RFI_{h10}, or RFI_{v10} indicates an anomalous emission from the ground transmitters and the occurrence of RFI at 6.925 and 10.65 GHz.

Figures 3a–c show spatial distributions of RFI over the United States. Areas of large positive RFI are indicated in red. A widespread RFI distribution at 6.925 GHz is found in the east and west coastal areas, including the cities of San Francisco and Los Angeles in west coastal California. High RFI values are also seen in the cities of Salt Lake City and Denver in the central western region. The east coast of the US is dominated by high RFI values at 6.925 GHz from Boston along the eastern corridor to New York, Baltimore, and Washington D. C. In most areas of Florida and Georgia, relatively few RFI sources are identified while the metropolitan region of Chicago is devoid of any RFI signal. However, there is nearly no RFI at 10.65 and 18.7 GHz over the US. Therefore, 10.65 GHz is assumed to be uncontaminated and is used as a "reference" value for developing the RFI detection and correction algorithms for the 6.925 GHz channel.

Overall, the RFI at 6.925 GHz over European and Asian continents (Fig. 4) is much sparser than that over the US. It is also seen that the RFI at 6.925 GHz does not spread out into other parts of Europe, including northern England. Different from the US, much of Europe is dominated by RFI at 10.65 GHz except for Turkey and northern Iran where RFI at 6.925 GHz is present. England and Italy have high negative RFI indices at 6.925 GHz. The amount of contamination varies from country to country in this region. For example, UK and Italy have very significant RFI while other countries, such as German, seem to have no RFI. The 6.925 GHz is taken as a "reference" over

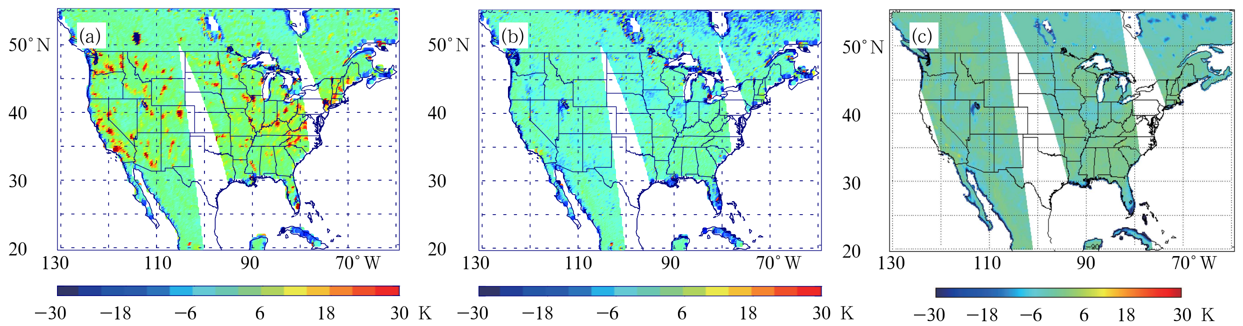

Fig. 3. AMSR-E RFI distribution in the US for the ascending node on 3 October 2008 at (a) 6.925, (b) 10.65, and (c) 18.7 GHz. Color scale units are in Kelvin.

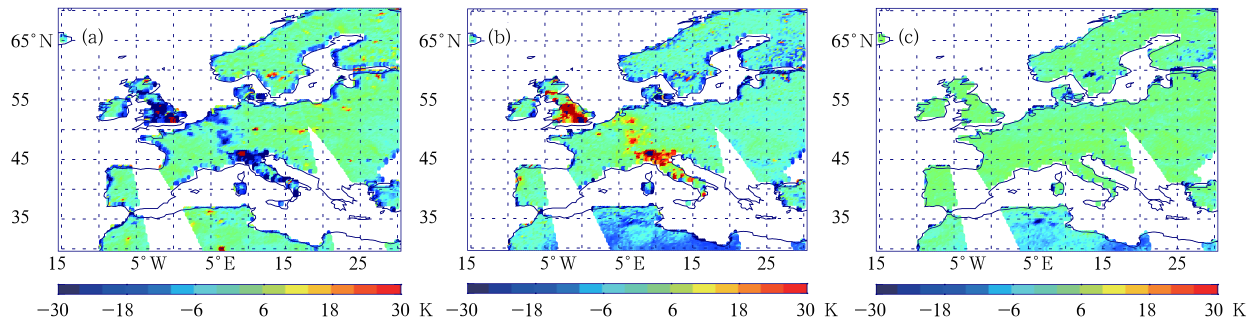

Fig. 4. AMSR-E RFI distribution in Europe for the ascending node on 3 October 2008 at (a) 6.925, (b) 10.65, and (c) 18.7 GHz. Color scale units are in Kelvin.

Europe.

RFI contaminations in Japan at both 6.925 and 10.65 GHz are shown in Fig. 5. RFI at 10.65 GHz is much more noticeable than that at 6.925 GHz. The 18.7 GHz is thus taken as a "reference" value for Japan.

The geographical difference of RFI seen above and the frequency-dependence of RFI can be explained from the spectrum allocations and protections imposed by the international organization. As shown in Appendix, in the US, the frequency at 6.925 GHz is unprotected for weather applications and has been used for commercial purposes whereas in the United Kingdom. The problem is more associated with 10.65 GHz.

The intensity of RFI signal is irregular from month to month but the RFI contamination tends to be stronger in larger cities. Figure 6 shows monthly RFI variability of two cities. The RFI was found to be widespread in both vertical and horizontal polarizations, appearing mostly near highly populated urban areas. The locations of the observed RFI were found to be persistent in time, but the magnitudes vary temporally and directionally (between ascending and descending passes). Although strong and moderate RFI could be identified, weak RFI is difficult to identify. This presents a challenge in designing a robust geophysical retrieval algorithm for which RFI-contaminated data must be identified and rejected.

In general, RFI maps generated from both ascending and descending passes are similar, and those from vertical and horizontal polarization data at these lower frequencies appear also quite similar. It is therefore difficult to relate the RFI distribution to the source of the interference signals from the RFI distribution information alone. The significant AMSR-E RFI occurs over a large proportion of the global land mass and is more intense at urban areas. At present, the affected frequencies are 6.925 and 10.65 GHz. The most likely source is from microwave communication links, with

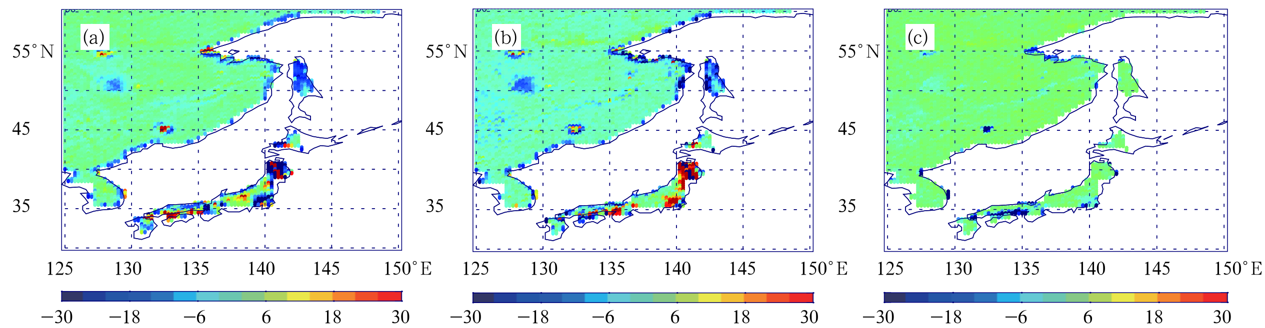

Fig. 5. AMSR-E RFI distribution in Japan for the ascending node on 3 October 2008 at (a) 6.925, (b) 10.65, and (c) 18.7 GHz. Color scale units are in Kelvin.

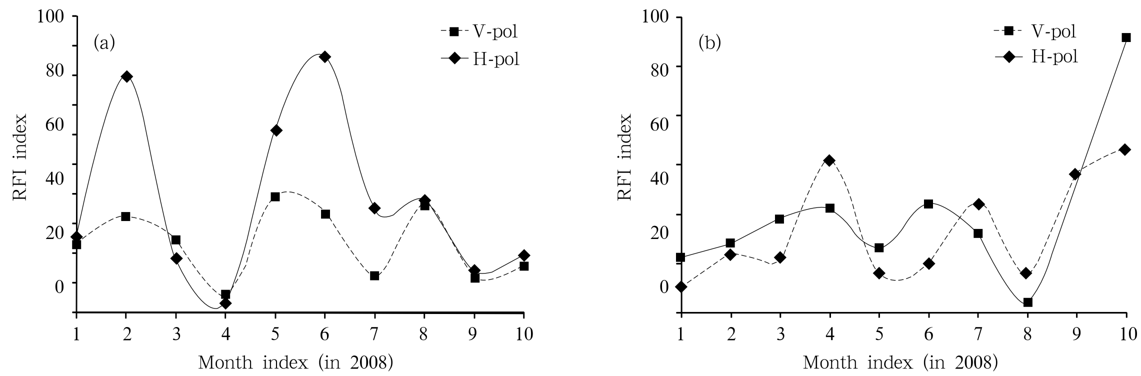

Fig. 6. Monthly RFI variability of two cities from January to October 2008 (1st day of each month). (a) RFI at 6.925 GHz in Washington D. C. and (b) RFI at 10.65 GHz in Rome. The dashed lines are for vertical polarization and the solid lines are for horizontal polarization.

regional legislation determining the main frequency.

Over oceans, occasional contaminations are also found and probably arise from some transportable sources onboard commercial ships and military cargos (Yan and Weng, 2008). At the RFI-free oceanic conditions, the AMSR-E brightness temperature at 10.65 GHz is normally higher than that at 6.925 GHz by more than a few degrees. This is due to the unique ocean surface emissivity spectra characteristic that the ocean emissivity increases with frequency. However, this nominal temperature gradient can be distorted by variable RFI sources so that the brightness temperature at 6.925 GHz is higher than that at 10.65 GHz by a few degrees.

4. RFI correction

Classification of AMSR-E RFI using the mean and standard deviation RFI index (see Eq. (1)) is effective in identifying strong RFI (Njoku et al., 2005). In many cases, however, it is difficult to use these indices to distinguish weak RFI from natural geophysical variability. Geophysical retrievals using RFI-filtered data may therefore contain residual errors due to the presence of data with weak RFI.

Of growing concern is the impact of RFI on assimilation of microwave imager data in land surface models. The residual RFI in the datasets could cause large biases in analysis and forecast fields of geophysical parameters such as soil moisture and land surface temperature. Therefore, a reliable RFI filter or mask needs to be further developed for improved microwave imager applications. A composite RFI index must be used from AMSR-E at the 6.925-GHz vertical polarization channel. The exact threshold indicates that the RFI intensity depends on radiometer sensitivity, frequencies and natural scene. Based on some mean emissivity spectral characteristics over various land types and after comparing simulated and observed brightness temperature spectra (i.e., Fig. 1), we derive the following composite RFI using two channels, i.e.,

$$\begin{aligned}&\mathrm{RFI}_{p,6} = \mathrm{TB}_{p,6} - \mathrm{TB}_{p,10}\\ &= \begin{pmatrix} 5-10\ \mathrm{K} & \text{weak} \\ 10-20\ \mathrm{K} & \text{moderate} \\ >20\ \mathrm{K} & \text{strong} \end{pmatrix}. \end{aligned} \tag{2}$$

In this study, the AMSR-E measurements over land with an RFI index greater than 5 K are defined as RFI-contaminated. Since the measurements at 18.7 GHz are rarely contaminated, if an RFI is detected at 10.65 GHz but not at 6.925 GHz, the RFI-contaminated AMSR-E measurements at 10.65 GHz are predicted from measurements at 18.7 or 6.925 GHz using two empirically-based equations which are derived using AMSR-E measurements under no-RFI contaminations. Also, if an RFI is detected at 6.925 GHz but not at 10.65 GHz, the RFI-contaminated measurements at 6.925 GHz can be predicted from measurements at 10.65 GHz. Again, when RFI contaminations are detected at both 6.925 and 10.65 GHz, RFI-contaminated measurements at these two frequencies still can be predicted from measurements at 18.7 GHz. Figure 7 presents a flow chart summarizing the entire decision tree process. Note that we have assumed that measurements at 18.7 GHz are nearly RFI-free (Njoku et al., 2004, 2005) Therefore, we can identify and correct the RFI-contamination when there is RFI at both 6.925- and 10.65-GHz frequencies.

When an RFI is detected at 6.925 GHz, the RFI-contaminated AMSR-E measurements at 6.925 GHz can be predicted from measurements at 10.65 GHz using four different algorithms which are derived using AMSR-E measurements under RFI-free conditions, as following:

$$\mathrm{TB}_{p,f_1} = a_0 + a_1\mathrm{TB}_{p,f_2}, \tag{3a}$$

$$\mathrm{TB}_{p,f_1} = a_0 + a_1\mathrm{TB}_{p,f_2} + a_2\mathrm{TB}^2_{p,f_2}. \tag{3b}$$

It is found that adding a quadratic term does not result in significant improvements in reducing biases and standard deviations. Thus, we use a linear form with dual polarizations to predict the brightness temperature from uncontaminated channels:

$$\mathrm{TB}_{p,f_1} = C_0 + C_1\mathrm{TB}_{\mathrm{H},f_2} + C_2\mathrm{TB}_{\mathrm{V},f_2}. \tag{4}$$

The coefficients in Eq. (4) and standard deviations are provided in Table 2.

By implementing the RFI correction algorithm, the anomalous brightness temperature spectrum is corrected and shown in Fig. 8. While the proposed algorithm reduces the RFI contamination significantly, there seems to be residual contamination around Los Angeles, central England, and particularly Tokyo.

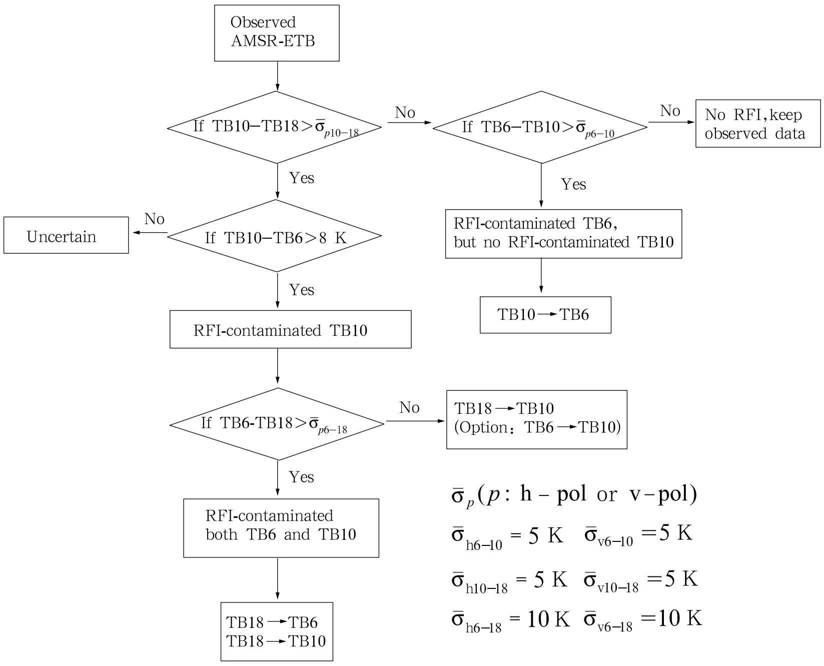

Fig. 7. RFI detection and correction algorithm flow chart.

Table 2. Coefficients and standard deviations of Eq. (4)

	p	f_1	f_2	C_0	C_1	C_2	STDEV
TB10→TB6	H-POL	6	10	–8.99197	0.951212	0.0752778	1.66425
	V-POL	6	10	–9.68610	–0.0718768	1.10629	1.53857
TB18→TB10	H-POL	10	18	9.31105	0.913560	0.0403827	1.29012
	V-POL	10	18	10.6396	–0.0904358	1.04417	1.48666
TB18→TB6	H-POL	6	18	17.4359	0.903253	0.0175537	2.21522
	V-POL	6	18	15.3020	–0.175613	1.11368	1.97212

Since weak RFI could not be easily distinguished from brightness temperature signals caused by natural geophysical variability, and it is difficult to differentiate between legitimate high values and contaminated high values, the residual contamination is acceptable. Empirical prediction based on other channel(s), while it often leads to clean images, sometimes fails to produce good quality retrieval of certain geophysical parameters where the image seems reasonable. The reason is that objects' specific signals are mistakenly removed as RFI contaminated signals.

Figure 9 shows scattering plots of two AMSR-E channels. The blue points within the pink oval-shaped are contaminated by RFI, and those with orange colors are the RFI-corrected data.

After the RFI correction, the TB bias compared to CRTM simulations is expected to reduce. The RFI-correction algorithm can produce a brightness temperature at AMSR-E frequencies with a root mean square (RMS) error of no more than 1.5 K. Moreover, the RFI-corrected AMSR-E observations can be used more efficiently in the retrieval of geophysical parameters of the earth and its atmosphere.

5. Summary and conclusions

Observation of the low-frequency microwave emissions is important for the retrieval of surface parameters such as soil moisture. However, AMSR-E measurements at low frequencies (6.925 and 10.65 GHz) over land are seriously contaminated by variable surface radio frequency transmitters. In order to properly

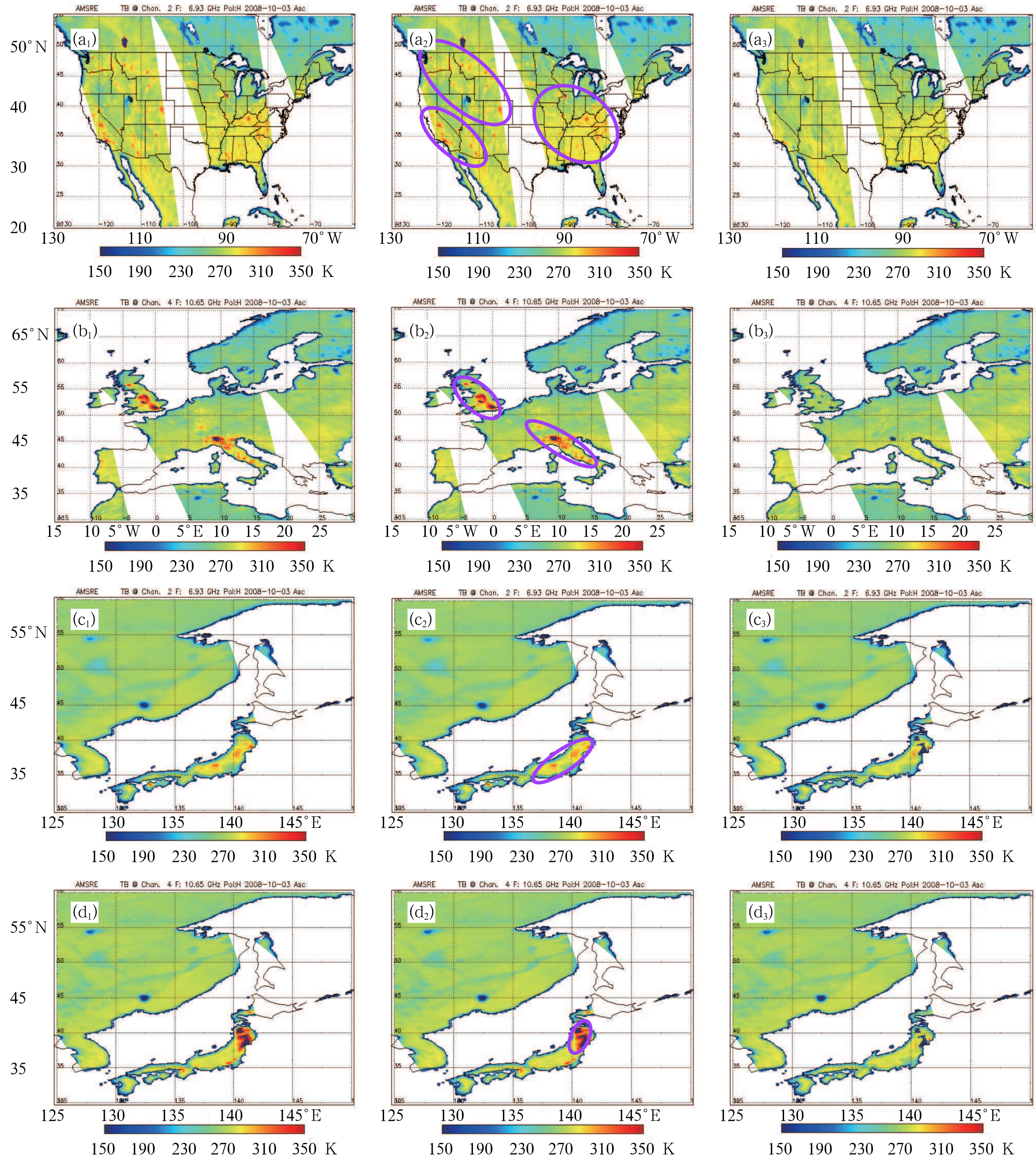

Fig. 8. Original and RFI corrected AMSR-E measurements on 3 October 2008. (a_1), (b_1), (c_1), and (d_1) are observed AMSR-E TB in US at 6.925 GHz, in UK at 10.65 GHz, in Japan at 6.925 GHz, and in Japan at 10.65 GHz, respectively. Circles in (a_2), (b_2), (c_2), and (d_2) denote areas identified as contaminated. (a_3), (b_3), (c_3) and (d_3) are RFI-corrected AMSR-E TB in US at 6.925 GHz, in UK at 10.65 GHz, in Japan at 6.925 GHz, and in Japan at 10.65 GHz, respectively. Color scale units are in Kelvin.

identify and reject increasing RFI contamination, an RFI identification and correction algorithm for AMSR-E channels is developed. It is based on mean emissivity spectral characteristics over various land types that are simulated using a microwave land emissivity model (Weng et al., 2001). RFI over land can be detected using an RFI index. The larger the RFI index is, the stronger the RFI contamination is. Since

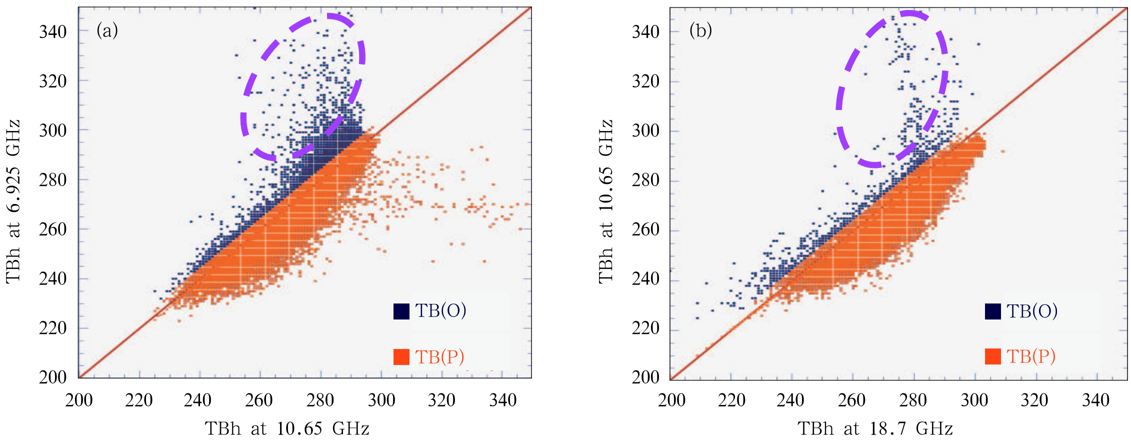

Fig. 9. AMSR-E channel relationship on 3 October 2008 at (a) 6.925 and 10.65 GHz and (b) 10.65 and 18.7 GHz. The data points with blue colors are the measurements and the circled points are RFI- contaminated ones. Those with orange colors are the RFI-corrected data.

measurements at 18.7 GHz are rarely contaminated, two empirically-based equations are derived using AMSR-E measurements under no-RFI contaminations. When an RFI is detected at 10.65 GHz, but not at 6.925 GHz, the RFI-contaminated AMSR-E measurements at 10.65 GHz are predicted from measurements at 18.7 or 6.925 GHz. When measurements at 6.925 GHz are contaminated by RFI, but not at 10.65 GHz, the RFI-contaminated AMSR-E measurements at 6.925 GHz are predicted from measurements at 10.65 GHz. When measurements at both 6.925 and 10.65 GHz are contaminated by RFI, measurements at 18.7 GHz are used to predict RFI for measurements at 6.925 and 10.65 GHz. With RFI mitigation, more RFI-contaminated AMSR-E measurements could be used for satellite data retrieval.

More robust radiometer designs and continued efforts to protect spectrum allocations will be needed in the future to ensure the viability of space borne passive microwave sensing. In addition, satellite sensors could be designed to detect RFI and enable RFI-contaminated data to be excised (Gasiewski et al., 2002; Ruf et al., 2006). For this purpose, it is necessary to design instruments with a relatively wide bandwidth in order to ensure that the amount of radiation received at the radiometer is measurable to a certain degree of accuracy.

APPENDIX

Radio Frequency Allocations

Frequency (GHz)	United States	United Kingdom	Europe	International
6.700–7.075	FIXED FIXED-SATELLITE (Earth-to-Space, Space-to-Earth) MOBILE	FIXED FIXED-SATELLITE (Earth to space) **UK102** MOBILE **UK111, UK143** **UK102** This Fixed-Satellite allocation is intended mainly for civil systems **UK111** Existing MoD Radiolocation systems may continue to operate NIB to essential civil services in accordance with T(F)(N)(80)5 **UK143** Electronic warfare calibration facilities operate on 7000 MHz	FIXED FIXED-SATELLITE (S/E)(E/S) EARTH EXPLORATION SATELLITE (passive) MOBILE	FIXED FIXED-SATELLITE (Earth-to-Space, Space-to-Earth) MOBILE
10.6–10.68	FIXED EARTH EXPLORATION SATELLITE (passive) SPACE RESEARCH (passive) RADIO ASTRONOMY	FIXED **UK125**, **UK127** EARTH EXPLORATION SATELLITE (passive) SPACE RESEARCH (passive) RADIO ASTRONOMY **UK125** aeronautical mobile **UK125** In the band 10·6–10·68 GHz the Fixed and Mobile except aeronautical mobile, services are limited to a maximum equivalent isotropic ally radiated power of 40·0 dBW. **UK126** The Radiolocation service is limited to: (1) Civil devices for indoor use only in the subband 10·675–10·699 GHz; (2) Military radars on NIB to the devices in (1) **UK127** The sub-bands 10·6–10·615 GHz and 10·64–10·68 GHz are used for civil communications including national defense circuits operated by public telecommunications operators	**10.6–10.65GHz** FIXED EARTH EXPLORATION SA TELLITE (passive) SPACE RESEARCH (passive) RADIO ASTRONOMY RADIO LOCATION MOBILE except aeronautical Mobile **10.65–10.68GHz** FIXED EARTH EXPLORATION SATELLITE (passive) SPACE RESEARCH (passive) RADIO ASTRONOMY RADIO LOCATION MOBILE except aeronautical	FIXED EARTH- EXPLORATION SATELLITE (passive) SPACE RESEARCH (passive) RADIO ASTRONOMY MOBILE except aeronautical mobile

18.6–18.8	FIXED-SATELLITE (Space-to-Earth) EARTH EXPLORATION SATELLITE (passive) SPACE RESEARCH (passive)	FIXED FIXED-SATELLITE (Space-to-Earth) EARTH EXPLORATION SATELLITE (passive) SPACE RESEARCH (passive) MOBILE except aeronautical mobile	FIXED FIXED-SATELLITE (S/E) EARTH EXPLORATION (passive) SPACE RESEARCH (passive) MOBILE except aeronautical	FIXED FIXED-SATELLITE (Space-to-Earth) EARTH EXPLORATION (passive) SPACE RESEARCH (passive) MOBILE except aeronautical mobile
23.6–24.0	EARTH EXPLORATION SATELLITE (passive) SPACE RESEARCH (passive) RADIO ASTRONOMY	EARTH EXPLORATION SATELLITE (passive) SPACE RESEARCH (passive) RADIO ASTRONOMY	EARTH EXPLORATION SATELLITE (passive) SPACE RESEARCH (passive) RADIO ASTRONOMY	EARTH EXPLORATION SATELLITE (passive) SPACE RESEARCH (passive) RADIO ASTRONOMY
36.0–37.0	FIXED EARTH EXPLORATION-SATELLITE (passive) SPACE RESEARCH (passive) MOBILE	FIXED EARTH EXPLORATION SATELLITE (passive) SPACE RESEARCH (passive) MOBILE	FIXED EARTH EXPLORATION SATELLITE (passive) SPACE RESEARCH (passive) RADIO MOBILE	FIXED EARTH EXPLORATION SATELLITE (passive) SPACE RESEARCH (passive) ASTRONOMY
86.0–92.0	EARTH EXPLORATION SATELLITE (passive) SPACE RESEARCH (passive) RADIO ASTRONOMY	EARTH EXPLORATION SATELLITE (passive) SPACE RESEARCH (passive) RADIO ASTRONOMY ***UK*146** Continuum measurements are conducted between 86.0–92.0 GHz	EARTH EXPLORATION SATELLITE (passive) SPACE RESEARCH (passive) RADIO ASTRONOMY	EARTH EXPLORATION SATELLITE (passive) SPACE RESEARCH (passive) RADIO ASTRONOMY

REFERENCES

Chauhan, N. S., S. Miller, and P. Ardanuy, 2003: Spaceborne soil moisture estimation at high resolution: a microwave-optical/IR synergistic approach. *Int. J. Remote Sens.*, **24**(22), 4599–4622.

Gasiewski, A. J., M. Klein, A. Yevgrafov, et al., 2002: Interference mitigation in passive microwave radiometry. *IEEE Geosci. Remote Sens. Symp. (IGARSS)*, 24–28.

Kawanishi, T., T. Sezai, Y. Ito, et al., 2003: The Advanced Microwave Scanning Radiometer for the Earth Observing System (AMSR-E), NASDA's contribution to the EOS for global energy and water cycle studies. *IEEE Trans. Geosci. Remote Sens.*, **41**(2), 184–194.

Kelly, R. E., A. T. Chang, L. Tsang, et al., 2003: A prototype AMSR-E global snow area and snow depth algorithm. *IEEE Trans. Geosci. Remote Sens.*, **41**(2), 230–242.

Li, L., E. G. Njoku, E. Im, et al., 2004: A preliminary survey of radio-frequency interference over the U.S. in Aqua AMSR-E data. *IEEE Trans. Geosci. Remote Sens.*, **42**(2), 380–390.

Njoku, E. G., and L. Li, 1999: Retrieval of land surface parameters using passive microwave measurements at 6–18 GHz. *IEEE Trans. Geosci. Remote Sens.*, **37**(1), 79–93.

——, W. J. Wilson, S. H. Yueh, et al., 2000: A large-antenna microwave radiometer-scatterometer concept for ocean salinity and soil moisture sensing. *IEEE Trans. Geosci. Remote Sens.*, **38**(6), 2645–2655.

——, T. J. Jackson, V. Lakshmi, et al., 2003: Soil moisture retrieval from AMSR-E. *IEEE Trans. Geosci. Remote Sens.*, **41**(2), 215–229.

——, T. Chan, W. Crosson, et al., 2004: Evaluation of the AMSR-E data calibration over land. *Int. J. Remote Sens.*, **30/31**, 19–38.

——, P. Ashcroft, T. K. Chan, and L. Li, 2005: Global survey and statistics of radio-frequency interference in AMSR-E land observations. *IEEE Trans. Geosci. Remote Sens.*, **43**(5), 938–947.

Owe, M., R. D. Jeu, and J. Walker, 2001: A methodology for surface soil moisture and vegetation optical depth retrieval using the microwave polarization difference index. *IEEE Trans. Geosci. Remote Sens.*, **39**(8), 1643–1654.

Paloscia, S., G. Macelloni, E. Santi, et al., 2001: A multi-frequency algorithm for the retrieval of soil moisture on a large scale using microwave data from SMMR and SSM/I satellites. *IEEE Trans. Geosci. Remote Sens.*, **39**(8), 1655–1661.

Ruf, C. S., S. M. Gross, and S. Misra, 2006: RFI detection and mitigation for microwave radiometry with an agile digital detector. *IEEE Trans. Geosci. Remote Sens.*, **44**(3), 694–706.

Weng, F. Z., B. H. Yan, and N. C. Grody, 2001: A microwave land emissivity model. *J. Geophys. Res.*, **106**(D17), 20115–20123, doi: 10.1029/2001JD900019.

Wilheit, T., C. D. Kummerow, and R. Ferraro, 2003: Rainfall algorithms for AMSR-E. *IEEE Trans. Geosci. Remote Sens.*, **41**(2), 204–214.

Yan, B. H., and F. Z. Weng, 2008: Application of AMSR-E measurements for tropical cyclone predictions. Part I: Retrieval of sea surface temperature and wind speed. *Adv. Atmos. Sci.*, **25**(2), 227–245.